Mean Field Analysis of Hypergraph Contagion Model

MEAN FIELD ANALYSIS OF HYPERGRAPH CONTAGION MODELS*

DESMOND JOHN HIGHAM† AND HENRY-LOUIS DE KERGORLAY‡

Abstract. We typically interact in groups, not just in pairs. For this reason, it has recently been proposed that the spread of information, opinion or disease should be modelled over a hypergraph rather than a standard graph. The use of hyperedges naturally allows for a nonlinear rate of transmission, in terms of both the group size and the number of infected group members, as is the case, for example, when social distancing is encouraged. We consider a general class of individual-level, stochastic, susceptible-infected-susceptible models on a hypergraph, and focus on a mean field approximation proposed in [Arruda et al., Phys. Rev. Res., 2020]. We derive spectral conditions under which the mean field model predicts local or global stability of the infection-free state. We also compare these results with (a) a new condition that we derive for decay to zero in mean for the exact process, (b) conditions for a different mean field approximation in [Higham and de Kergorlay, Proc. Roy. Soc. A, 2021], and (c) numerical simulations of the microscale model.

Key words. compartmental, collective contagion, epidemiology, spectral analysis, susceptible-infected-susceptible.

AMS subject classifications. 92D30, 60J27

1. Motivation and Background. Biological and social contagion processes can be used to model the way that opinions, rumours, ideas or diseases propagate through a community [9, 17]. Traditionally a graph, or network, is used to represent the possible routes for person-to-person transmission [11, 14, 22, 26]. Recent work has suggested that it is beneficial to account directly for the higher-order group structures that arise in human-to-human interactions, using hypergraphs [7, 15, 20] or simplicial complexes [16, 24, 25]. Indeed, beyond-pairwise interactions are also relevant in many other social, economic and technological settings [1, 2, 3, 4, 10].

In the context of opinion dynamics, an individual may be affected differently if multiple members of the same group (such as a workplace or household) express a view than if the same number of contacts from different groups express that view [16]; this is an example of a *majority effect* [18]. Similarly, in the spread of a disease, having multiple infected contacts in the same group may lead to a different infection rate than having the same number of contacts across independent groups [20]. For example, (unknowingly) sharing a photocopier with four infected colleagues may not be four times as risky as sharing it with one infected colleague, if the item is cleaned regularly. On the other hand, if there is a viral load threshold [8] then sharing a car with four infected colleagues may be more than four times as risky as sharing a car with one infected colleague. Moreover the overall group size may have an effect—for a fixed classroom space, there may be a cutoff on the number students beyond which attempts at social distancing become ineffective.

For these reasons, it is natural to consider a model of spreading that (a) uses information about the groups present, rather than simply the resulting pairwise interactions, and (b) allows for the transmission rate to be a nonlinear function of

* **Funding:** Both authors were supported by Engineering and Physical Sciences Research Council grant EP/P020720/1. DJH was also supported by Engineering and Physical Sciences Research Council grant EP/W011093/1.

†School of Mathematics, University of Edinburgh, Edinburgh, EH9 3FD, UK (d.j.higham@ed.ac.uk).

‡School of Mathematics, University of Edinburgh, Edinburgh, EH9 3FD, UK (hdekerg@ed.ac.uk)

the number of active individuals. Particular nonlinearities of interest are the concave, or *collective suppression*, case [15] and the threshold, or *collective contagion*, case [7, 15, 16, 20]. This leads to the hypergraph-based model that we describe in section 2, and the mean field approximation from [7] that we describe in section 3. Sections 4 and 5 give stability analysis for the exact and mean field processes, respectively. In section 6 we compare results with those for an alternative mean field model of [15]. An unusual feature of the mean field model in [7] is that although it takes the form of a deterministic ODE system with real-valued components, it evaluates the nonlinear infection rate function only at non-negative integer arguments, just as the exact stochastic model does. This feature complicates the analysis, but we show that it offers benefits when the nonlinearity is concave. Illustrative computational experiments are described in section 7. Corresponding results for a more general and flexible version of the hypergraph-based model are given in section 8, and conclusions appear in section 9.

To be concrete, we describe the models and analysis in the language of epidemiology, but we emphasize that the concepts and results are relevant in other scenarios.

The main contributions of this work are:

- for the exact model: a condition that guarantees decay to zero in mean of the infection level (Theorem 4.3) and, for concave nonlinearity, a condition that guarantees exponential decay to zero of the disease level (Theorem 6.1),
- for the mean field model of [7]: a condition for local asymptotic stability of the disease-free state (Theorem 5.1), and conditions for global asymptotic stability of the disease-free state with collective suppression and collective infection nonlinearities (Theorems 5.2 and 5.3),
- extensions for the mean field model associated with a more general multi-type model where the nonlinear infection rate may depend on the type and size of the hyperedge (Theorems 8.1, 8.2 and 8.3).

2. Notation and Individual-level Model. Before describing the model, we first introduce some definitions and notation.

A *hypergraph* [6] is a generalization of graph in which an edge, now called a *hyperedge*, may join any number of vertices. More formally, a hypergraph is a is a tuple $\mathcal{H} := (V, E)$, where V is a set of vertices and E is a set of nonempty subsets of V which specifies the hyperedges.

We denote the number of nodes and hyperedges by n and m, respectively; that is, $|V| = n$ and $|E| = m$. Assuming that the vertices and hyperedges have been ordered in some (arbitrary) way, we use $\mathcal{I}$ to denote the corresponding *incidence matrix*; here $\mathcal{I} \in \mathbb{R}^{n\times m}$ has $\mathcal{I}_{ih} = 1$ if node i belongs to hyperedge h and $\mathcal{I}_{ih} = 0$ otherwise.

In our context the vertices represent individuals in a population of size n, and the hyperedges record group interactions. For example, a set of vertices may form a hyperedge if the corresponding individuals live in the same household, work in the same office or sing in the same choir.

Following the original idea in [5], which has also been studied in [7, 16], we use a continuous time Markov process to track the propagation of disease through the population in a susceptible-infected-susceptible (SIS) framework. The state vector $X(t) \in \mathbb{R}^n$ is such that $X_i(t) = 1$ if vertex i is infected at time t and $X_i(t) = 0$ otherwise.

We assume that the instantaneous recovery rate is given by a constant $\delta > 0$, and we let $\lambda_i(X(t))$ denote the state-dependent instantaneous infection rate for vertex i,

given $X(t)$; that is,

$$\mathbb{P}\left(X_i(t+\varepsilon)=1 \,|\, X(t)\right) = \begin{cases} \lambda_i(X(t))\,\varepsilon + o(\varepsilon), & \text{if } X_i(t)=0, \\ 1-\delta\,\varepsilon + o(\varepsilon), & \text{if } X_i(t)=1, \end{cases} \tag{2.1}$$

and

$$\mathbb{P}\left(X_i(t+\varepsilon)=0 \,|\, X(t)\right) = \begin{cases} \delta\,\varepsilon + o(\gamma), & \text{if } X_i(t)=1, \\ 1-\lambda_i(X(t))\,\varepsilon + o(\varepsilon), & \text{if } X_i(t)=0. \end{cases} \tag{2.2}$$

In this way, specifying the model reduces to defining the infection rates, $\lambda_i(X(t))$. We mention that in the standard graph setting [11, 22, 26], where interactions involve only pairs of vertices, $\lambda_i(X(t))$ is taken to be proportional to the number of infected neighbours of vertex i at time t. Hence, in that case, the infection rate is linear in the number of infected neighbours. As discussed in section 1, we are interested in the setting of group interactions and possibly nonlinear infection rates.

Now, writing X_j rather than $X_j(t)$ for convenience, we will assume that for a given vertex i, the contribution to the overall infection rate from a given hyperedge h is

$$\beta\,\mathcal{I}_{ih}\,f(\sum_{j=1}^{n}\mathcal{I}_{jh}X_j). \tag{2.3}$$

Here, when $\mathcal{I}_{ih}=1$, so that i is a member of the hyperdge, the argument passed to the function f is the number of infected individuals to which i is exposed in this hyperedge. Hence f describes the dependence of the infection rate on the number of infected individuals. The disease cannot spread unless there is at least one infected individual in the hyperedge, so we may assume throughout that $f(0)=0$. The factor β in (2.3) represents the inherent infectiousness of the disease.

For example, consider a one-hour meeting between a predefined group of co-workers (forming a hyperedge) that takes place in a dedicated meeting room. Suppose further that, for this size of meeting room, five infected individuals, but no fewer, generate sufficient viral load to pass on the infection (perhaps through airborne microdroplets or through indirect contact). Then a suitable nonlinearity in (2.3) could be $f(x)=c\,\max\{0,x-4\}$ or $f(x)=c\,\mathbb{1}(x\geq 5)$, for some constant c; these are of collective contagion form [7, 15, 16, 20]. Now suppose that the meeting room is in continual use, for different groups (hyperedges) within the workforce, and that vertex i may participate in several meetings. We may then take the sum of (2.3) over all groups (hyperedges).

For the purpose of analysis, it will be useful to distinguish between hyperedges according to their size, so we have classes $\mathcal{C}_2,\dots,\mathcal{C}_K$ with $h\in\mathcal{C}_k \Leftrightarrow |h|=k$. Then the overall infection rate for vertex i may be written

$$\lambda_i(X(t)) = \beta\sum_{k=2}^{K}\sum_{h\in\mathcal{C}_k}\mathcal{I}_{ih}\,f(\sum_{j=1}^{n}\mathcal{I}_{jh}X_j). \tag{2.4}$$

It is also natural to generalize the expression (2.4) to incorporate different types of hyperedge; for example these may correspond to groups that congregate in various sizes of classroom, workspace, residence, or vehicle, and groups that interact through various kinds of sports or leisure activities. Each different type of hyperedge may

be given its own function f to quantify the dependence of the infection rate on the number of infected individuals in that setting, and $\lambda_i(X(t))$ in (2.4) would generalize to include the sum over all contributions. The analysis below extends readily to this case, at the expense of notational complexity. For the sake of clarity, we therefore state and prove results for the one-type model (2.4), and in Section 8 we explain how the results extend to the multi-type model.

In [7] the authors considered a model of the form (2.1), (2.2), (2.4) with a particular collective contagion nonlinearity f. (More precisely, the model in [7] is covered by the multi-type setting of Section 8.) A first order, or mean field, approximation to the individual-level model was derived in [7], and the dynamical behaviour of the resulting ODE system was investigated numerically. In the next section we describe this mean field approach for a general nonlinearity, f. Later, in section 6, we compare the performance of this model with another, simpler, mean field approximation that was derived and studied in [15] based on the idea of commuting the order of $\mathbb{E}$ and f.

3. Mean Field Hypergraph Models. The rate of infection expressed in (2.4) is random. To make large-scale simulations tractable, and to facilitate analysis, it is natural to focus on the evolution of the the expected processes $(p_i(t))_{t\geq 0} := (\mathbb{E}[X_i(t)])_{t\geq 0}$, $i \in \{1, 2, \ldots, n\}$. Substituting the random rates of infection by their expectation, gives

$$\frac{dp_i}{dt} = \mathbb{E}[\lambda_i(X(t))](1 - p_i) - \delta p_i. \tag{3.1}$$

Taking expected values in (2.4), the expected rate of infection may be written

$$\begin{aligned} \mathbb{E}[\lambda_i(X(t))] &= \beta \sum_{k=2}^{K} \sum_{h \in \mathcal{C}_k} \mathcal{I}_{ih} \mathbb{E}[f(\sum_{j=1}^{n} X_j \mathcal{I}_{jh})] \\ &= \beta \sum_{k=2}^{K} \sum_{h \in \mathcal{C}_k} \mathcal{I}_{ih} \sum_{l=1}^{k} f(l) \mathbb{P}(\sum_{j=1}^{n} X_j \mathcal{I}_{jh} = l). \end{aligned} \tag{3.2}$$

This expression defines the expected rate exactly, but it does not appear to be amenable to numerical simulation. In [7], an approximation was introduced by assuming independence of the X_j, giving

$$\mathbb{P}(\sum_{j=1}^{n} X_j \mathcal{I}_{jh} = l) \approx \Psi(h, l) := \sum_{J_l \subset h} \prod_{j \in J_l} p_j \prod_{j \in h \setminus J_l} (1 - p_j), \tag{3.3}$$

where J_l runs over all possible subsets of nodes of hyperedge h, of size l. To avoid cumbersome notation, we do not explicitly denote the dependence of p_j on t or the dependence of $\Psi(h, l)$ on the p_j. With this approximation, the expected processes $P(t) := (p_i(t))_{i=1}^n$ satisfy the deterministic ODE system

$$\frac{dP(t)}{dt} = g(P(t)), \tag{3.4}$$

where $g : \mathbb{R}^n \to \mathbb{R}^n$ is defined by

$$g_i(P(t)) := \beta \sum_{k=2}^{K} \sum_{h \in \mathcal{C}_k} \mathcal{I}_{ih} (\sum_{l=1}^{k} f(l) \Psi(h, l))(1 - p_i(t)) - \delta p_i(t). \tag{3.5}$$

We emphasize that, with a slight abuse of notation, $p_i(t)$ is now being used to denote a mean field approximation to $\mathbb{E}[X_i(t)]$. We also note that the factors $\mathcal{I}_{ih}$ in (3.5) implicitly depend on k through the hyperedge constraint $h \in \mathcal{C}_k$. To make the model physically reasonable we assume that the initial conditions satisfy $0 \le p_i(0) \le 1$ for $i = 1, \ldots, n$, and we note that $0 \le p_i(t) \le 1$ for $i = 1, \ldots, n$ then follows for all $t > 0$.

This mean field ODE was derived and studied numerically in [7] with an emphasis on first-and second-order transitions, bistability and hysteresis. Our aim in this work is to derive analytical results that address a more fundamental question: under what conditions will the disease will die out? We do this by studying the local and global stability of the disease-free state. In the next section, we show that it is possible to analyse the exact expected process, and in section 5 we move on to the mean field approximation (3.4)–(3.5).

4. The Exact Expected Process. Here we show that, while the exact equation describing the dynamics of the expected processes (3.1) does not seem to be amenable to numerical simulation, an upper bound argument allows us to derive vanishing conditions. In the following analysis, and throughout the remaining sections, we define the symmetric matrix $W \in \mathbb{R}^{n\times n}$ by

$$W_{ij} := \sum_{k=2}^{K} \sum_{h\in\mathcal{C}_k} \mathcal{I}_{ih}\mathcal{I}_{jh}, \tag{4.1}$$

so that W_{ij} records the number of hyperedges containing both nodes i and j. Given a symmetric matrix A, we let $\lambda(A)$ denote its largest eigenvalue. Recall from (3.1) and (3.2) that we have, for $i \in \{1, 2, \ldots, n\}$,

$$\frac{dp_i}{dt} = \beta(1-p_i) \sum_{k=2}^{K} \sum_{h\in\mathcal{C}_k} \mathcal{I}_{ih}\mathbb{E}[f(X_j\mathcal{I}_{jh})] - \delta p_i. \tag{4.2}$$

We also define the constant

$$c_f := \max_{\{k\in\{1,2,\ldots,K\}\,|\,\mathcal{C}_k \text{ nonempty}\}} \frac{f(k)}{k}.$$

We then have

$$\begin{aligned}\beta \sum_{k=2}^{K} \sum_{h\in\mathcal{C}_k} \mathcal{I}_{ih}\mathbb{E}[f(\sum_{j=1}^{n} X_j\mathcal{I}_{jh})] &\le \beta\, c_f \sum_{k=2}^{K} \sum_{h\in\mathcal{C}_k} \mathcal{I}_{ih} \sum_{j=1}^{n} p_j\mathcal{I}_{jh} \\ &= \beta\, c_f \sum_{j=1}^{n} W_{ij}p_j.\end{aligned}$$

Hence, from (4.2), we have the following differential inequalities, for $i \in \{1, 2, \ldots, n\}$,

$$\frac{dp_i}{dt} \le c_f\, \beta \sum_{j=1}^{n} W_{ij}p_j(1-p_i) - \delta p_i. \tag{4.3}$$

To analyse this system of differential inequalities, we first state a result that has been proved for scalar problems.

THEOREM 4.1 ([23]). *Suppose that u satisfies the scalar ordinary differential inequality $du(t)/dt \leq f(u(t), t)$ and y satisfies the scalar ODE $dy(t)/dt = f(y(t), t)$, with boundary condition $u(t_0) = y(t_0)$. Then*

$$\begin{cases} \forall\ t < t_0,\ u(t) \geq y(t) \\ \forall\ t > t_0,\ u(t) \leq y(t). \end{cases}$$

This result extends naturally to systems of differential inequalities as follows.

THEOREM 4.2. *Suppose that $\{u_i\}_{i=1}^n$ satisfies the system of ordinary differential inequalities*

$$\forall\ i \in \{1, 2, \ldots, n\},\ \forall\ t \in \mathbb{R},\ \frac{du_i(t)}{dt} \leq f_i(u(t), t),$$

that $\{y_i\}_{i=1}^n$ satisfies the ODE system

$$\forall\ i \in \{1, 2, \ldots, n\},\ \forall\ t \in \mathbb{R},\ \frac{dy_i(t)}{dt} = f_i(y(t), t),$$

and that for all $i \in \{1, 2, \ldots, n\}$, $u_i(t_0) = y_i(t_0)$. Then for all $i \in \{1, 2, \ldots, n\}$

$$\begin{cases} \forall\ t < t_0,\ u_i(t) \geq y_i(t) \\ \forall\ t > t_0,\ u_i(t) \leq y_i(t). \end{cases}$$

For our purposes, we have the following.

COROLLARY 4.1. *If for all $i \in \{1, 2, \ldots, n\}$, $du_i(t)/dt \leq g_i(u(t))$, $dy_i(t)/dt = g_i(y(t))$ and $u_i(0) = y_i(0)$, then for all $i \in \{1, 2, \ldots, n\}$ and all $t \geq 0$, $u_i(t) \leq y_i(t)$.*

We are interested in finding conditions under which the spread of the disease predicted by (4.2) vanishes as $t \to \infty$. By Corollary 4.1 and (4.3), it suffices to find such conditions for the following, more simple, model

$$\frac{dP(t)}{dt} = \widetilde{g}(P(t)), \tag{4.4}$$

where $\widetilde{g} : \mathbb{R}^n \to \mathbb{R}^n$ is defined by

$$\widetilde{g}_i(P(t)) := \beta\, c_f \sum_{j=1}^{n} W_{ij} p_j(t)(1 - p_i(t)) - \delta p_i(t). \tag{4.5}$$

This system can be analysed by appealing to [15, Theorem 6.4] in the case where the infection function is the identity (which, in particular, is concave), and we deduce the following result.

THEOREM 4.3 (Extinction in mean for the exact process). *If*

$$\frac{\beta\, c_f\, \lambda(W)}{\delta} < 1, \tag{4.6}$$

then 0 is a globally asymptotically stable equilibrium for (4.4) and hence for (4.2), that is, for all $i \in \{0, 1, \ldots, n\}$ and all initial conditions, $\lim_{t\to\infty} p_i(t) = 0$ in (4.2).

Considering the collective suppression case, where f is concave and $f(0) = 0$, we have for all $x \in \mathbb{N}$, $f(x) \leq f(1)x$; hence $c_f = f(1)$.

For a collective contagion model of the form $f(x) := c_2\,\mathbb{1}(x \geq c_1)$ for some constants $c_1 \geq 1$ and $c_2 > 0$, we have for all $x \in \mathbb{N}$, $f(x) \leq c_2\,x/c_1$, hence $c_f \leq c_2/c_1$.

Theorem 4.3 gives a practical condition for the exact model that guarantees decay to zero in mean of the infection level of every component. In the next section we seek similar results for the mean field approximation (3.4)–(3.5). This allows us (a) to judge the accuracy of this mean field approximation in terms of a corresponding spectral threshold, and (b) to get insights into the behaviour of a system that can be simulated directly. Also, in section 6 we use this analysis to compare predictions against those of the alternative mean field model from [15].

5. Analysis of Mean Field Hypergraph Model. Here we analyze the mean field model described in (3.4)–(3.5). We find conditions for local and global asymptotic stability of the disease-free state of the process, considering various assumptions on the infection function f, including collective contagion and collective suppression cases. Our first result is a spectral condition for local asymptotic stability.

THEOREM 5.1 (General condition for local asymptotic stability). *If*

$$\frac{\beta\,f(1)\,\lambda(W)}{\delta} < 1, \tag{5.1}$$

then $0 \in \mathbb{R}^n$ is a locally asymptotically stable equilibrium for (3.4)–(3.5).

Proof. We have $g(0) = 0$ in (3.4)–(3.5), so $0 \in \mathbb{R}^n$ is an equilibrium. Recall the standard result that local asymptotic stability follows if every eigenvalue of the Jacobian matrix $\nabla g(0)$ has a negative real part. For $j_0 \neq i$ we compute

$$\frac{\partial g_i}{\partial p_{j_0}} = \beta \sum_k \sum_{h \in \mathcal{C}_k} \mathcal{I}_{ih}\mathcal{I}_{j_0 h} \sum_{l=1}^{k} f(l) \frac{\partial \Psi}{\partial p_{j_0}}(h,l)(1-p_i), \tag{5.2}$$

and along the diagonal

$$\frac{\partial g_i}{\partial p_i} = \beta \sum_k \sum_{h \in \mathcal{C}_k} \mathcal{I}_{ih} \sum_{l=1}^{k} f(l) \frac{\partial \Psi}{\partial p_i}(h,l)(1-p_i) - \beta \sum_k \sum_{h \in \mathcal{C}_k} \mathcal{I}_{ih} \sum_{l=1}^{k} f(l)\Psi(h,l) - \delta. \tag{5.3}$$

We see that $\nabla g(0) = B - \delta I$, where

$$B_{ij} := \beta \sum_k \sum_{h \in \mathcal{C}_k} \mathcal{I}_{ih}\mathcal{I}_{jh} \sum_{l=1}^{k} f(l) \frac{\partial \Psi}{\partial p_j}(h,l)|_{P=0}.$$

Let $h \in E$ be a hyperedge, let $j_0 \in V = \{1, 2, \ldots, n\}$ be a node of the hypergraph, and let $\tilde{h} := h \setminus \{j_0\}$. Using (3.3), we find

$$\frac{\partial \Psi(h,l)}{\partial p_{j_0}} = \mathcal{I}_{j_0 h} \left(\sum_{J_{l-1} \cup \{j_0\} \subset h} \prod_{j \in J_{l-1}} p_j \prod_{j \in \tilde{h} \setminus J_{l-1}} (1-p_j) - \sum_{J_l \subset \tilde{h}} \prod_{j \in J_l} p_j \prod_{j \in \tilde{h} \setminus J_l} (1-p_j) \right)$$

and hence

$$\frac{\partial \Psi(h,l)}{\partial p_{j_0}}|_{P=0} = \mathcal{I}_{j_0 h}\delta_{l1},$$

with Kronecker delta notation, so that $\delta_{xy} = 1$ if $x = y$, and $\delta_{xy} = 0$ otherwise. It follows that $B_{ij} = \beta f(1) \sum_{k=2}^{K-1} \sum_{h \in \mathcal{C}_k} \mathcal{I}_{ih}\mathcal{I}_{jh} = \beta f(1) W_{ij}$.

We see that $\nabla g(0)$ is symmetric and $\lambda(\nabla g(0)) = \lambda(B - \delta I) = \lambda(W)f(1)\beta - \delta$. So it suffices for local asymptotic stability that $\lambda(W)f(1)\beta/\delta < 1$, as stated. ∎

The above result has the advantage that it does not require specific assumptions on the infection model. However, it is relevant only when the initial proportion of infected individuals is sufficiently small. We now consider particular infection models, with the aim of constructing a global asymptotic stability result. As discussed in section 2, and in more detail in [15], two cases of practical relevance are: a *collective suppression model*, characterized by a concave infection function f, and a *collective contagion model*, characterized by $f(i) = 0$ for $i = 0, 1, \ldots, m-1$ with some $m \geq 2$. In the latter case, the disease may only start spreading in a hyperedge if the number of infected individuals in that hyperedge reaches a critical threshold value, m. When the infection function is concave, the local asymptotic stability result obtained in Theorem 5.1 extends to the case of global asymptotic stability.

THEOREM 5.2 (Global asymptotic stability for a collective suppression model). *Suppose that f is concave. If the spectral bound (5.1) holds, then $0 \in \mathbb{R}^n$ is globally asymptotically stable for (3.4)–(3.5).*

To prove this theorem, we first introduce a few preliminary results. Let $h \in E$ be a hyperedge. To avoid cumbersome notation we assume that $|h| = K$ and let the nodes in h be $\{1, 2, \ldots, K\}$. Any other hyperedge could be analyzed in similar way, but, for example, in Lemma 5.2 below we would then need to write $\{1, 2, \ldots, K\} \setminus \{i\}$ rather than $\{1, 2, \ldots, K-1\}$. Also, to streamline the presentation, we use the additional notation $[K] = \{1, 2, \ldots, K\}$ where convenient.

We seek to estimate the spectrum of the Jacobian matrix of g at all points $P \neq 0$. Hence, from (5.2)–(5.3), we need to estimate $\displaystyle\sum_{l=1}^{k} f(l)\frac{\partial \Psi}{\partial p_K}(h, l)$. To this end, let us first rewrite $\Psi(h, l)$ according to the following lemma.

LEMMA 5.1. *Let $\{z_i\}_{i=1}^K$ be a set of independent Bernoulli random variables such that for each $i \in \{1, 2, \ldots, K\}$*

$$z_i = \begin{cases} 1 & \text{with probability } p_i \\ 0 & \text{with probability } 1 - p_i. \end{cases}$$

For every $l \in \{1, 2, \ldots, K\}$

$$\mathbb{P}(\sum_{i=1}^{K} z_i = l) = \sum_{J_l \subset [K]} \prod_{j \in J_l} p_j + \sum_{k=l+1}^{K} (-1)^{k-l} \binom{l+k}{l} \sum_{J_k \subset [K]} \prod_{j \in J_k} p_j,$$

where J_l runs over all possible subsets of $[K] := \{1, 2, \ldots, K\}$ of size l.

Proof. Letting $A_i := \{z_i = 1\}$ for every $i \in [K]$, we have for $l \in [K]$

$$\mathbb{P}(\sum_{i=1}^{K} z_i = l) = \sum_{J_l \subset [K]} \mathbb{P}\left((\cap_{i \in J_l} A_i) \cap (\cap_{j \in [K] \setminus J_l} A_j^c) \right), \tag{5.4}$$

where A^c denotes the complement of event A.

Let us estimate $\mathbb{P}(A \cap A_{l+1}^c \cap \cdots \cap A_K^c)$, where $A := A_1 \cap \cdots \cap A_l$, thus considering without loss of generality the case $J_l = [l]$. Define the induced probability measure from A by

$$\mathbb{P}_A(B) := \frac{\mathbb{P}(A \cap B)}{\mathbb{P}(A)}.$$

By the inclusion-exclusion principle, we have

$$\begin{aligned}
&\mathbb{P}(A \cap A_{l+1}^c \cap \cdots \cap A_K^c) \\
&= \mathbb{P}(A)\mathbb{P}_A(A_{l+1}^c \cap \cdots \cap A_K^c) \\
&= \mathbb{P}(A)\left(1 - \sum_{i=l+1}^{K} \mathbb{P}_A(A_i) + \right. \\
&\qquad \left. \sum_{l+1 \le i < j \le K} \mathbb{P}_A(A_i \cap A_j) + \cdots + (-1)^{K-l}\mathbb{P}_A(A_{l+1} \cap \cdots \cap A_K)\right) \\
&= \mathbb{P}(A) - \sum_{i=l+1}^{K} \mathbb{P}(A \cap A_i) \\
&\quad + \sum_{l+1 \le i < j \le K} \mathbb{P}(A \cap A_i \cap A_j) + \cdots + (-1)^{K-l}\mathbb{P}(A \cap A_{l+1} \cap \cdots \cap A_K).
\end{aligned}$$

Spanning over all J_l, we see that for each $i \in \{l+1, \ldots, K\}$, $\mathbb{P}(A \cap A_i)$ is substracted in (5.4) exactly $l+1$ times. Indeed it is counted once for each J_l satisfying

$$\begin{aligned}
&\exists\ i_0 \in [K] \setminus J_l,\ (\cap_{j \in J_l} A_j) \cap A_{i_0} = A \cap A_i = A_1 \cap \cdots \cap A_l \cap A_i \\
\Leftrightarrow\ &\exists\ i_0 \in [K] \setminus J_l,\ J_l \cup \{i_0\} = \{1, 2, \ldots, l, i\},
\end{aligned}$$

which yields $\binom{l+1}{l} = l+1$ possible choices for J_l. Likewise, for every $1 \le i < j \le K$, $\mathbb{P}(A \cap A_i \cap A_j)$ is added exactly $\binom{l+2}{l}$ times in (5.4), and more generally every $(-1)^{k-l}\mathbb{P}(A \cap A_{j_{l+1}} \cap \ldots A_{j_k})$ is added in (5.4) exactly $\binom{l+k}{l}$ times. This, together with the independence of the z_i, yields the claimed formula. ∎

Using Lemma 5.1, we deduce the following lemma.

LEMMA 5.2. *We have*

$$\sum_{l=1}^{K} f(l)\frac{\partial \Psi}{\partial p_K}(h,l) = f(1) + \sum_{k=2}^{K-1} x_k \Big(\sum_{J_{k-1} \subset [K-1]} \prod_{j \in J_{k-1}} p_j \Big),$$

where, for $k \ge 2$, we let

$$x_k := f(k) + \sum_{l=1}^{k-1} (-1)^l \binom{2k-l}{k-l} f(k-l). \tag{5.5}$$

Proof. By Lemma 5.1, we can rewrite $\Psi(h,l)$ as

$$\Psi(h,l) = \sum_{J_l \subset [K]} \prod_{j \in J_l} p_j + \sum_{k=l+1}^{K} (-1)^{k-l} \binom{l+k}{l} \sum_{J_k \subset [K]} \prod_{j \in J_k} p_j. \tag{5.6}$$

From (5.6), we find for $K \ge 2$ (for $K = 1$, the partial derivative is equal to 1) that

$\partial\Psi(h,l)/\partial p_K$ takes the form

$$\begin{cases} 1+\sum_{k=1}^{K-1}(-1)^k\binom{l+k+1}{l}\sum_{J_k\subset[K-1]}\prod_{j\in J_k}p_j, & \text{if } l=1 \\ \sum_{J_{l-1}\subset[K-1]}\prod_{j\in J_{l-1}}p_j+\sum_{k=l}^{K-1}(-1)^{k-l+1}\binom{l+k+1}{l}\sum_{J_k\subset[K-1]}\prod_{j\in J_k}p_j, & \text{otherwise.} \end{cases}$$

Multiplying the above by $f(l)$, summing over l and grouping the terms according to each $\sum_{J_k\subset[K-1]}\prod_{j\in J_k}p_j$, we find that

$$\sum_{l=1}^{K}f(l)\frac{\partial\Psi}{\partial p_K}(h,l)$$

may be written

$$f(1)\ +\ \sum_{k=2}^{K-1}(f(k)+\sum_{l=1}^{k-1}(-1)^l\binom{2k-l}{k-l}f(k-l))(\sum_{J_{k-1}\subset[K-1]}\prod_{j\in J_{k-1}}p_j).$$ ∎

LEMMA 5.3. *Suppose that f is concave, then $x_k\le 0$ in (5.5) for all $k\ge 2$.*

Proof. It is clear that $x_2\le 0$, so it remains to show that $x_k\le 0$ for all $k\ge 3$. Letting $C_l:=\binom{2k-l}{k-l}$ for fixed $k\ge 3$, we have

$$\sum_{l=1}^{k-1}(-1)^l C_l f(k-l)=$$
$$\begin{cases} -\left((C_1f(k-1)-C_2f(k-2))+\cdots+C_{k-1}f(1)\right), & k\equiv 0 \bmod 2 \\ -\left((C_1f(k-1)-C_2f(k-2))+\cdots+(C_{k-2}f(2)-C_{k-1}f(1))\right), & k\equiv 1 \bmod 2. \end{cases}$$

Since $C_lf(k-l)$ is decreasing in l, it suffices to show, for all $k\ge 3$, that

$$f(k)\le\begin{cases} C_{k-1}f(1)=(k+1)f(1), & k\equiv 0 \bmod 2 \\ C_{k-2}f(2)-C_{k-1}f(1)=\binom{k+2}{2}f(2)-(k+1)f(1), & k\equiv 1 \bmod 2. \end{cases}$$

By the concavity of f and $f(0)=0$, we see that the slopes $f(k)/k$ are decreasing in $k\ge 1$. Hence we already have that $f(k)\le(k+1)f(1)$, and it remains to show that for all $k\ge 3$

$$f(k)\le\binom{k+2}{2}f(2)-(k+1)f(1).$$

Dividing both sides of the above inequality by k, we see that the LHS decreases in k, while the RHS increases in k; hence it suffices to show the inequality for $k=3$. By the concavity of f, $f(3)\le 2f(2)-f(1)$, hence $\binom{5}{2}f(2)-4f(1)\ge 4f(3)$. ∎

Proof of Theorem 5.2. From the global asymptotic stability result in [13, Lemma 1′] it is sufficient to show that all eigenvalues of the symmetric matrix

$$(\nabla g(P))^{(S)} := (\nabla g(P) + \nabla g(P)^T)/2$$

are strictly less than 0, for all $P \neq 0$.

From (5.2)–(5.3), using Lemma 6.3 in [15] with diagonal matrix given by $\Lambda_{ii} := \beta \sum_k \sum_{h \in \mathcal{C}_k} \mathcal{I}_{ih} \sum_{l=1}^{k} f(l)\Psi(h,l) \geq 0$, we deduce that

$$\lambda(\nabla g(P)^{(S)}) \leq \lambda(B^{(S)} - \delta I),$$

where $B_{ij} := \beta \sum_k \sum_{h \in \mathcal{C}_k} \mathcal{I}_{ih}\mathcal{I}_{jh} \sum_{l=1}^{k} f(l) \dfrac{\partial \Psi}{\partial p_j}(h,l)(1-p_i)$.

Since f is concave, we know by Lemmas 5.2 and 5.3, that for all $1 \leq j \leq n$, $\sum_{l=1}^{K} f(l) \dfrac{\partial \Psi}{\partial p_j}(h,l) \leq f(1)$, from which it follows that

$$0 \leq B_{ij}^{(S)} \leq \beta f(1) \sum_{k=2}^{K-1} \sum_{h \in \mathcal{C}_k} \mathcal{I}_{ih}\mathcal{I}_{jh} = \beta f(1) W_{ij}.$$

Hence $\lambda((\nabla g(P))^{(S)}) \leq \lambda(\beta f(1) W - \delta I)$, and it suffices that $\lambda(W)\dfrac{f(1)\beta}{\delta} < 1$, which completes the proof of Theorem 5.2. ∎

Applying Lemmas 5.2 and 5.3 to the identity function (which is concave), we find

$$\sum_{l=1}^{K} l \frac{\partial \Psi(h,l)}{\partial p_K} \leq 1.$$

Hence for all choices of f, if $c_f > 0$ is such that for all $x \in \mathbb{N}$, $f(x) \leq c_f x$, then

$$\sum_{l=1}^{K} f(l) \frac{\partial \Psi(h,l)}{\partial p_K} \leq c_f \sum_{l=1}^{K} l \frac{\partial \Psi(h,l)}{\partial p_K} \leq c_f.$$

In particular for a collective infection model, where $f(x) := c_2 \mathbb{1}(x \geq c_1)$, we deduce that

$$\sum_{l=1}^{K} f(l) \frac{\partial \Psi(h,l)}{\partial p_K} \leq \frac{c_2}{c_1},$$

from which the next theorem follows.

THEOREM 5.3 (Global asymptotic stability for a collective contagion model). *Suppose that $f(x) := c_2 \mathbb{1}(x \geq c_1)$. If*

$$\frac{\beta\, c_2\, \lambda(W)}{\delta\, c_1} < 1, \tag{5.7}$$

then $0 \in \mathbb{R}^n$ is globally asymptotically stable for (3.4)–(3.5).

The proof of Theorem 5.2 above may be used to establish this result, substituting $f(1)$ by c_2/c_1 everywhere.

6. Comparison with Alternative Mean Field Model and Exact Model. As mentioned in section 2, an alternative mean field approximation model was introduced and studied in [15]. This is given by

$$\frac{dP(t)}{dt} = \widehat{g}(P(t)), \tag{6.1}$$

where $\widehat{g}_i : \mathbb{R}^n \to \mathbb{R}$ is defined by

$$\widehat{g}_i(P(t)) := \beta \sum_{h \in E} \mathcal{I}_{ih} f\left(\sum_{j=1}^{n} p_j(t)\mathcal{I}_{jh}\right)(1 - p_i(t)) - \delta p_i(t). \tag{6.2}$$

The key approximation in the derivation of this model is to take the expectation operation inside the function f. Comparing (3.4)–(3.5) and (6.1)–(6.2), one major difference is that while the infection function f is only evaluated over integers in g, it is evaluated on a continuous domain in $\widehat{g}$. This leads to different factors in the spectral bounds. Indeed, suppose that f is concave. Theorem 5.2 tells us that the solution of the mean field approximation model given by g in (3.4)–(3.5) vanishes if $\beta\, f(1)\, \lambda(W)/\delta < 1$. For the model defined by $\widehat{g}$ in (6.1)–(6.2), [15, Theorem 6.4] gives the condition

$$\frac{\beta\, f'(0)\, \lambda(W)}{\delta} < 1 \tag{6.3}$$

for global asymptotic stability. In this concave setting, the slopes $x \mapsto (f(x) - f(0))/(x - 0)$ are decreasing in $x > 0$. Since $f(0) = 0$, we deduce that $f'(0) = \lim_{x \to 0} f(x)/x \geq f(1)$ always holds true. Hence, for the mean field model (3.4)–(3.5) we have *a less restrictive sufficient condition* for vanishing of the disease. Moreover, the following theorem shows that a similar condition controls the behavior of the exact solution, and hence, in this sense, (3.4)–(3.5) gives a more accurate approximation than (6.1)–(6.2) in the concave case.

THEOREM 6.1. *Suppose that f is concave in the mean field model given by (3.4)–(3.5). Also assume for simplicity that each node has the same, independent, initial infection probability denoted by i_0; that is, for $j = 1, 2, \ldots, n$,*

$$\mathbb{P}(X_j(0) = 1) = i_0. \tag{6.4}$$

Then

$$\mathbb{P}\left(\sum_{i=1}^{n} X_i(t) > 0\right) \leq n\, i_0\, \exp\left((\beta\, f(1)\, \lambda(W) - \delta)t\right).$$

Hence, if $\beta\, f(1)\, \lambda(W)/\delta < 1$ the disease vanishes at an exponential rate.

Proof. This result may be proved using the arguments in the proof of [15, Theorem 8.1], noticing that we can substitute $f'(0)$ by $f(1)$. ∎

The following corollary also holds, analogously to [11] and [15, Corollary 8.2], where $f'(0)$ is again replaced by $f(1)$.

COROLLARY 6.1. *Suppose f is concave in the mean field model given by (3.4)–(3.5). Let τ denote the time of extinction of the disease and suppose $\beta\, f(1)\, \lambda(W)/\delta < 1$. Then*

$$\mathbb{E}[\tau] \leq \frac{1 + \log n}{\delta - \beta\, f(1)\, \lambda(W)}.$$

7. Computational Experiments. In this section we report on results of computational experiments that allow us to test the sharpness of the results derived in section 5, and also allow us to compare the two mean field models that we have discussed against each other and against the exact stochastic model.

7.1. Simulation algorithm. First, let us summarize our approach for the mean field approximation (3.4)–(3.5). We use the discrete Fourier representation of $\Psi(h,l)$ derived in [7] to render the computation of (3.5) more stable. We solve the ODE systems (3.4)–(3.5) and (6.1)–(6.2) with Euler's method, using a time step $\Delta t = 0.05$.

For the exact stochastic model, defined by (2.1), (2.2) and (2.4), we use the discretization approach described in [15]. More precisely, to advance from time t to $t+\Delta t$ we first let $r \in [0,1]^n$ be a random vector of i.i.d. values uniformly sampled from $[0,1]$. Then for $1 \le i \le n$,

- when $X_i(t) = 0$, we set $X_i(t+\Delta t) = 1$ if
$$r_i < 1 - \exp\left(-\lambda_i(X(t))\Delta t\right),$$
and we set $X_i(t+\Delta t) = 0$ otherwise;
- when $X_i(t) = 1$, we set $X_i(t+\Delta t) = 0$ if
$$r_i < 1 - \exp\left(-\delta \Delta t\right),$$
and we set $X_i(t+\Delta t) = 1$ otherwise.

For these computations we also used $\Delta t = 0.05$.

The number of nodes is chosen to be $n = 400$, and hyperedges of prescribed sizes are generated independently by choosing nodes uniformly at random. In Figure 7.1, 7.2, 7.3, 7.4, and 7.5, there are 400 edges, 200 hyperedges of size 3, 100 hyperedges of size 4 and 50 hyperedges of size 50. The sizes and number of hyperedges differ in Figure 7.6, 7.7 and 7.8, and are specified in the descriptions of the figures.

7.2. Experimental Comparisons. In Figures 7.1, 7.2, 7.3, 7.4 and 7.5, we compare the time evolution of the two mean field models (3.4)–(3.5) and (6.1)–(6.2), with the exact model. The figures show the proportion of infected individuals: $\sum_{j=1}^{n} X_j(t)/n$ for the exact model and $\sum_{j=1}^{n} p_j(t)/n$ for the mean field models. The exact model was run 100 times independently. The solid green envelopes represent the span of the runs: at each time point we discard the most extreme 10% of the values; that is, 5% of the values above and below the average. In these plots, we used the same initial infection probability i_0 for each node, as in (6.4). The figures give results for different i_0 and β values. In all figures, we label the y-axis by i, indicating the proportion of infected individuals over time for Figures 7.1-7.4, and the proportion of infected individuals at a fixed time T in Figures 7.5-7.8.

Figures 7.1 and 7.2 use concave infection rates of $\arctan(x)$ and $\log(1+x)$, respectively. Here, both mean field models are seen to give good qualitative approximations to the exact models, but it is noticeable that the model (6.1)–(6.2) (red dashed line), which applies continuous-valued arguments to f, overestimates the infection level when β and i_0 are small and hence the disease vanishes over time.

Figure 7.3 uses another concave infection rate, $f(x) = \min\{3, x\}$. Here, both mean field models substantially overestimate the infection level for small β and i_0. It is intuitively reasonable that the two mean field models behave similarly in this example,

since on hyperedges of size less than or equal to 4 the infection rate function is linear, and hence commutes with the expectation operation.

In Figure 7.4, we consider a partitioned collective contagion model defined as follows. Letting f_k denote the infection rate function applied to all hyperedges of size $k+1$, we let $f_1 : x \mapsto x$, and $f_k : x \mapsto c_{2,k}\mathbb{1}(x \geq c_{1,k})$, $k \in \{2, \ldots, 4\}$. Here we chose $c_{1,k} = c_{2,k} := k - 1$, for $k \in \{2, \ldots, 4\}$. In this case, the mean field model (3.4)–(3.5) (purple dots) fails to predict decay of the disease for small β and i_0.

In Figure 7.5 we directly compare the accuracy with which the mean field models predict disease outbreak, as a function of β, and we also test the sharpness of the spectral bounds. Here we use the concave infection rates $2\log(1+x)$ and arctan. The vanishing conditions predicted by the spectral bounds (5.1) and (6.3), yielding the green vertical lines in Figure 7.5, occur at $\beta_1 \cong 0.0369$ and $\beta_2 \cong 0.0268$ respectively for $f(x) = 2\log(1+x)$, and at $\beta_1 \cong 0.0629$ and $\beta_2 \cong 0.0494$ respectively, for $f(x) = \arctan(x)$. With initial infection probability $i_0 = 0.5$ we averaged the infection level at $T = 200$ over 10 runs. Blue crosses correspond to the exact model. We see both mean field models are conservative in the sense that they give growth for β values where the exact model produces no infection. The figures also show the spectral bounds on β arising from (5.1) and (6.3) as vertical lines, and we see that they give sharp predictions.

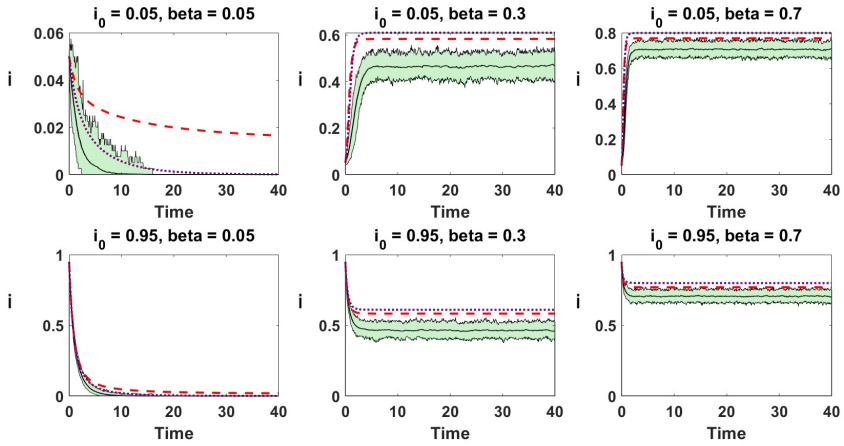

FIGURE 7.1. *Proportion of infected individuals, i, over time. Infection function $f(x) = \arctan(x)$. Purple dots: mean field approximation from (3.4)–(3.5). Red dashed line: mean field approximation from (6.1)–(6.2). Black solid line: mean of the individual-level stochastic model.*

7.3. Collective contagion model: sensitivity to the initial condition. An interesting working assumption is that only hyperedges of size three or greater are present, and hence there are no pairwise interactions. This circumstance may arise, for example, if we restrict attention to a workplace or school environment. Here we check how this assumption may impact the predictive performance of the two mean field models, in the case of collective contagion. We used the same infection rate functions as in Figure 7.4. In Figures 7.6, 7.7, and 7.8, we show, for both mean field models and the exact stochastic model, the proportion of infected individuals at time $T = 100$ averaged over 5 runs, as a function of the initial proportion i_0 of infected individuals.

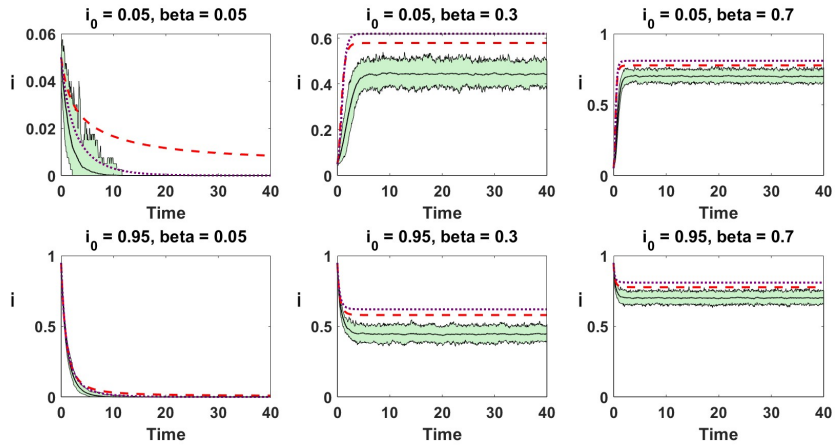

FIGURE 7.2. *Proportion of infected individuals, i, over time. Infection function $f(x) = \log(1+x)$. Purple dots: mean field approximation from (3.4)–(3.5). Red dashed line: mean field approximation from (6.1)–(6.2). Black solid line: mean of the individual-level stochastic model.*

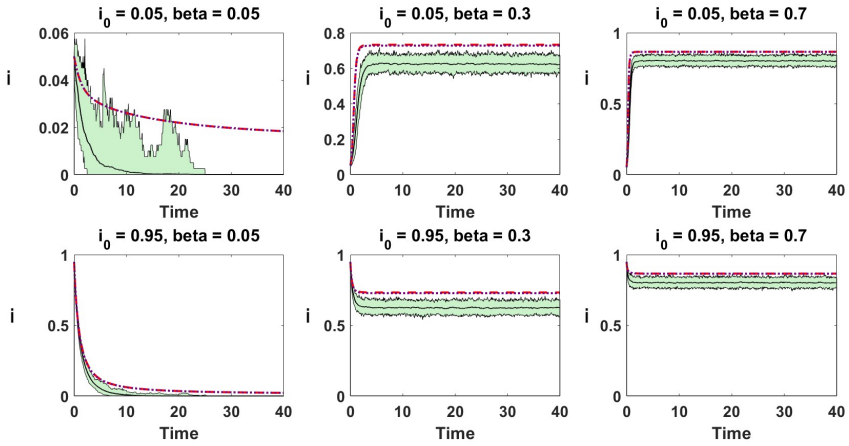

FIGURE 7.3. *Proportion of infected individuals, i, over time. Infection function $f(x) = \min\{3, x\}$. Purple dots: mean field approximation from (3.4)–(3.5). Red dashed line: mean field approximation from (6.1)–(6.2). Black solid line: mean of the individual-level stochastic model.*

We observe that the mean field model given by (3.4)–(3.5) remains relatively stable, while the behaviour of the mean field model given by (6.1)–(6.2) appears to be sensitive to the initial condition i_0, its predictive performance degrading if i_0 is small (e.g., red dots in Figure 7.6). This sensitivity can be understood intuitively by recalling that the model in (3.4)–(3.5) is expressed as a continuous function of $P \in \mathbb{R}^n$, while the model in (6.1)–(6.2) is expressed in terms of step functions of the form $\mathbb{1}(\sum_i p_i \mathcal{I}_{ih} \leq c_1)$; the later are not continuous functions of P and are more sensitive to small perturbations of the initial condition. Furthermore, for initial value $P(0) = (i_0)_{i=1}^n$ sufficiently small

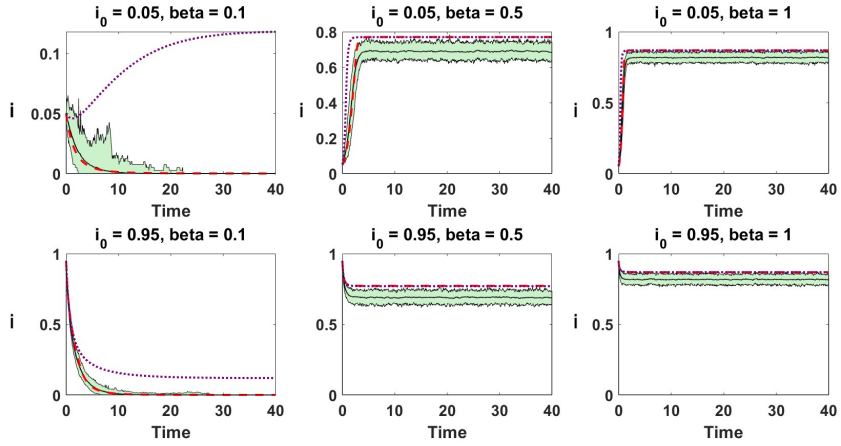

FIGURE 7.4. *Proportion of infected individuals, i, over time. Collective contagion partitioned model. Purple dots: mean field approximation from (3.4)–(3.5). Red dashed line: mean field approximation from (6.1)–(6.2). Black solid line: mean of the individual-level stochastic model.*

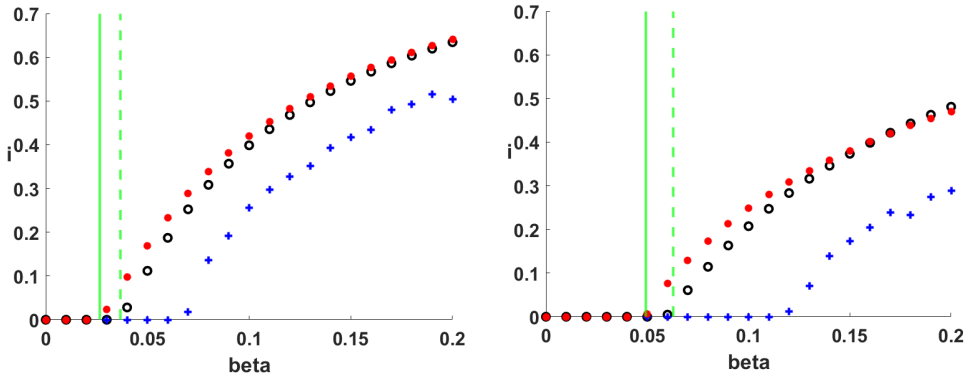

FIGURE 7.5. *Infection function* $2\log(1+x)$ *(left) and* $\arctan$ *(right). Horizontal axis is infection strength,* β*. Vertical axis is the proportion of infected individuals at time* $T = 200$ *for the two mean field approximations, (6.1)–(6.2) (red dots) and (3.4)–(3.5) (black circles), and for the individual-level stochastic model (blue crosses), averaged over* 10 *runs. The spectral bounds on* β *from (5.1) and (6.3) relating to the two mean field approximations, are shown respectively as a solid green vertical line (below which the red dots must be* 0*) and a dashed green vertical line (below which the black circles must be* 0*).*

that the threshold conditions of the above step functions are not satisfied, the infection rate expressed by (6.1)–(6.2) will remain zero, while the infection may start to spread according to the other models, thus yielding an underestimate of the propagation of the virus in the population.

We note that if the number of hyperedges is relatively low compared with the number of nodes (as in Figure 7.8), then the exact model will not propagate, in which case the mean field model given by (6.1)–(6.2) will give a better prediction. However, we see that both mean field models fail to accurately predict the behaviour of the

model for sufficiently large initial condition i_0.

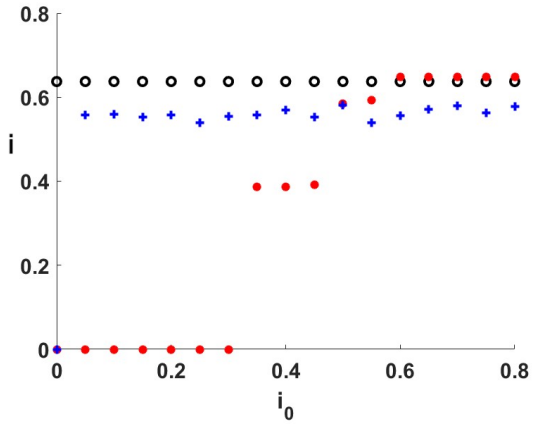

FIGURE 7.6. *Proportion of infected individuals, i, at time $T = 100$ for the two mean field approximation models (red dots for (6.1)–(6.2) and black circles for (3.4)–(3.5)) and the individual-level stochastic model (blue crosses). Using* 200 *hyperedges of size* 3, 100 *hyperedges of size* 4, 50 *hyperedges of size* 5 *for* 400 *nodes.*

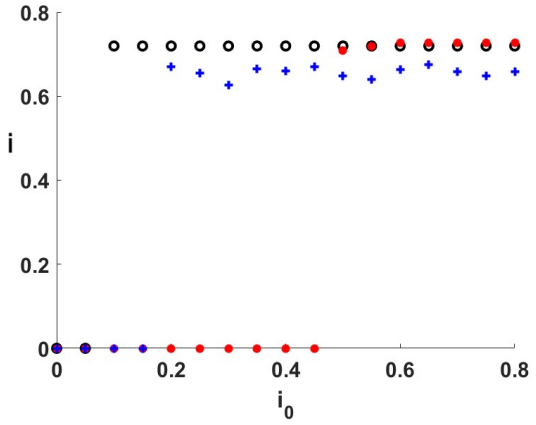

FIGURE 7.7. *Proportion of infected individuals, i, at time $T = 100$ for the two mean field approximation models (red dots for (6.1)–(6.2) and black circles for (3.4)–(3.5)) and the individual-level stochastic model (blue crosses). Using* 200 *hyperedges of size* 4, 100 *hyperedges of size* 5 *for* 400 *nodes.*

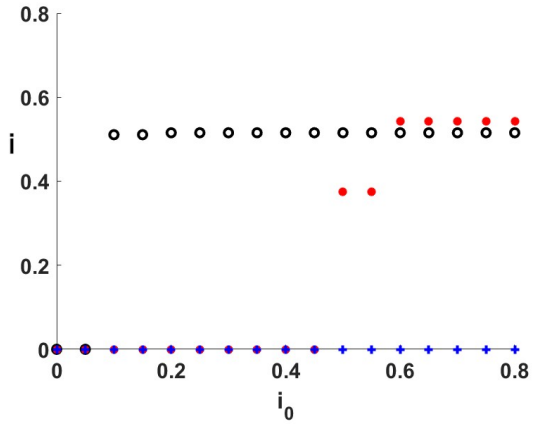

FIGURE 7.8. *Proportion of infected individuals, i, at time $T = 100$ for the two mean field approximation models (red dots for (6.1)–(6.2) and black circles for (3.4)–(3.5)) and the individual-level stochastic model (blue crosses). Using* 100 *hyperedges of size* 4, 50 *hyperedges of size* 5 *for* 400 *nodes.*

8. Multi-type Model. In the above results, we assumed for simplicity that a fixed infection function f applies for all hyperedges. The results, however, readily extend to a *multi-type partition model*, where the infection rate function may depend on the type and size of the hyperedge. As we discussed in section 2, the classes of hyperedge may correspond to locations, such as households, schools, offices, shops and public transport vehicles, and hyperedge size may have an impact on transmission if individuals are attempting to mutually distance. We will therefore explain how the main results change when we extend the infection rate model. Let us partition the hyperedges of the hypergraph into S disjoint families $\{\mathcal{F}_s\}_{s=1}^{S}$, such that to each family $\mathcal{F}_s$ corresponds an infection function f_s. For each $s \in \{1, 2, \dots, S\}$ we may further partition the hyperedges in $\mathcal{F}_s$ into disjoint classes $\mathcal{C}_2^{(s)}, \dots, \mathcal{C}_{K_s}^{(s)}$, where a hyperedge $h \in \mathcal{F}_s$ belongs to $\mathcal{C}_k^{(s)}$ if and only if $|h| = k$. The infection rate model (2.4) may then be extended to

$$\lambda_i(X(t)) = \beta \sum_{s=1}^{S} \sum_{k=2}^{K_s} \sum_{h \in \mathcal{C}_k^{(s)}} \mathcal{I}_{ih}^{(s),(k)} f_s\Big(\sum_{j=1}^{n} \mathcal{I}_{jh}^{(s),(k)} X_j\Big), \tag{8.1}$$

where $\mathcal{I}^{(s),(k)}$ is the incidence matrix inducing the subhypergraph spanned by the hyperedges of $\mathcal{C}_k^{(s)} \subset \mathcal{F}_s$, i.e., $\mathcal{I}_{ih}^{(s),(k)} = 1$ if $h \in \mathcal{C}_k^{(s)} \subset \mathcal{F}_s$ and $i \in h$, and $\mathcal{I}_{ih}^{(s),(k)} = 0$ otherwise. We then have the following generalization of the ODE system in (3.4)–(3.5)

$$\frac{dP(t)}{dt} = g(P(t)), \tag{8.2}$$

where $g : \mathbb{R}^n \to \mathbb{R}^n$ is defined by

$$g_i(P(t)) = \beta \sum_{s=1}^{S} \sum_{k=2}^{K_s} \sum_{h \in \mathcal{C}_k^{(s)}} \mathcal{I}_{ih}^{(s),(k)} \Big(\sum_{l=1}^{k} f_s(l) \Psi(h, l)\Big)(1 - p_i(t)) - \delta p_i(t). \tag{8.3}$$

Define also $\mathcal{I}^{(s)} := \sum_{k=2}^{K_s} \mathcal{I}^{(s),(k)}$ to be the incidence matrix inducing the subhypergraph

spanned by the hyperedges in $\mathcal{F}_s$, and let $W^{(s)} := \mathcal{I}^{(s)}(\mathcal{I}^{(s)})^T$, so that $W^{(s)}_{ij}$ records the number of hyperedges in $\mathcal{F}_s$ containing both i and j. We then have the following results for the generalized partition model, which are extensions of Theorems 5.1, 5.2 and 5.3.

THEOREM 8.1 (General condition for local asymptotic stability). *If*

$$\frac{\beta\,\lambda\left(\sum_{s=1}^{S} f_s(1)W^{(s)}\right)}{\delta} < 1, \tag{8.4}$$

then $0 \in \mathbb{R}^n$ is a locally asymptotic stable equilibrium for (8.2)–(8.3).

THEOREM 8.2 (Global asymptotic stability for a collective suppression model). *Suppose that f_s is concave for all $s \in \{1, 2, \ldots, S\}$. If (8.4) holds, then $0 \in \mathbb{R}^n$ is globally asymptotically stable for (8.2)–(8.3).*

THEOREM 8.3 (Global asymptotic stability for a collective contagion model). *Suppose that for each $s \in \{1, 2, \ldots, S\}$, $f_s(x) := c_{2,s}\mathbb{1}(x \geq c_{1,s})$, where $c_{1,s} \geq 2$ and $c_{2,s} > 0$. If*

$$\frac{\beta\,\lambda\left(\sum_{s=1}^{S} \frac{c_{2,s}}{c_{1,s}} W^{(s)}\right)}{\delta} < 1,$$

then $0 \in \mathbb{R}^n$ is globally asymptotically stable for (8.2)–(8.3).

9. Summary and Conclusions. Hypergraphs offer more flexibility and realism than pairwise, graph-based models and they are relevant to many spreading processes where members of a population form groups. In the pairwise setting, with linear infection rates, graph-based models have been widely studied, and spectral stability bounds derived [11, 14, 22, 26]. Spectral analysis for the hypergraph case was initially developed in [15], both for an exact individual-level stochastic model and a deterministic mean field approximation. In this work we focused on a more sophisticated mean field approximation that was proposed in [7] and requires a more detailed analysis. Although this ODE system produces real-valued trajectories, it has the unusual feature of evaluating the nonlinear infection rate function only at integer arguments. Intuitively, since the infection function is zero at the origin, this feature is likely to make the approximation more accurate than the version in [15] in the case of concave nonlinearity and small infection levels. This behaviour was observed in our computational tests (Figures 7.1–7.3 and Figure 7.5) and is backed by our theoretical analysis—in the concave case, this mean field model produces a locally asymptotically stable disease-free state under the same condition as the exact model (see Theorem 4.3 with $c_f = f(1)$ and Theorem 5.2). However, for other types of nonlinear infection rate, it is possible for the mean field model in [15] to give a better approximation (Figure 7.4). Hence a key conclusion from this work is that both mean field models can be analysed rigorously and both can provide useful information. A second conclusion is that the matrix W in (4.1) is an informative flattening of a hypergraph in terms of predicting stability of the infection-free state. We may view W as the weighted adjacency matrix associated with the clique expansion of the hypergraph, and we mention that recent work [21] has argued that the "expansion eigenvalue" $\lambda(W)$ is also useful for relating hypergraph assortative mixing patterns to other dynamical processes. We note that in many settings W will be a more convenient and less invasive quantity to measure or estimate than the overall hypergraph interaction structure: asking an individual for a list of their contacts and the number of distinct group-level interactions they have

with these contacts is less demanding and intrusive than asking for complete details of all their group memberships.

It is notable that the spectral conditions for decay of the disease level appearing in our results have the form

$$\frac{\beta\, c\, \lambda(W)}{\delta} < 1,$$

for some constant c that is determined by the type of nonlinear infection rate (with generalized versions in section 8). This expression separates out different aspects of the process in a natural manner and offers a means to inform mitigation strategies. The parameters β and δ quantify the inherent infectiousness and recovery rate for the disease, respectively. The constant c is affected by the way that the chance of a new infection depends on the number of infected people in a group. This could be controlled by changing behavioural patterns; for example, through face-covering or social distancing. The factor $\lambda(W)$ summarizes the interaction structure. Lockdown measures that restrict movement and therefore limit physical encounters will have the effect of reducing the size of the nonnegative integer entries in W. It follows from the Perron-Frobenius theorem that if the resulting matrix is irreducible, then $\lambda(W)$ will have been *strictly* reduced. Hence lockdown has a tangible effect on the spectral bound. It would of course be interesting to characterise $\lambda(W)$ for various classes of hypergraph and to derive results that quantify more precisely the effect on $\lambda(W)$ of removing hyperedges.

On a practical level, it would also be of interest to calibrate a hypergraph model against real data and investigate the predictive power of the spectral bounds that we have derived.

Finally, we note that hypergraph epidemic models have also been studied with regard to the analysis of bifurcation phenomena. It was found in particular in [7] that the collective contagion model exhibits bistability and hysteresis. More generally, it was shown in [19] that any generic additional parameter variation can cause a transformation from a second-order to a first-order transition phase at a critical point. This was illustrated in particular with adaptive epidemic dynamics ([12, 19]). Given such an additional parameter for adaptive hypergraphs, and a particular choice of the nonlinear infection function f, if the global stability condition for the disease free state fails before the local condition (5.1) does, this would suggest the existence of a discontinuous transition.

Data Statement MATLAB code for the experiments described here may be found at `https://www.maths.ed.ac.uk/~dhigham/algfiles.html`

REFERENCES

[1] U. Alvarez-Rodriguez, F. Battiston, G. F. de Arruda, Y. Moreno, M. Perc, and V. Latora, *Evolutionary dynamics of higher-order interactions in social networks*, Nat. Hum. Behav., (2021).

[2] F. Battiston, G. Cencetti, I. Iacopini, V. Latora, M. Lucas, A. Patania, J.-G. Young, and G. Petri, *Networks beyond pairwise interactions: Structure and dynamics*, Physics Reports, 874 (2020), pp. 1–92.

[3] A. R. Benson, R. Abebe, M. T. Schaub, A. Jadbabaie, and J. Kleinberg, *Simplicial closure and higher-order link prediction*, Proceedings of the National Academy of Sciences, 115 (2018), pp. E11221–E11230.

[4] A. R. Benson, D. F. Gleich, and J. Leskovec, *Higher-order organization of complex networks*, Science, 353 (2016), pp. 163–166.

[5] A. Bodó, G. Katona, and P. Simon, *SIS epidemic propagation on hypergraphs*, Bulletin of Mathematical Biology, 78 (2016), pp. 713–735.

[6] A. Bretto, *Hypergraph Theory: An introduction*, Springer, Berlin, 2013.
[7] G. F. de Arruda, G. Petri, and Y. Moreno, *Social contagion models on hypergraphs*, Phys. Rev. Res., 2 (2020).
[8] M.-A. de La Vega, G. Caleo, J. Audet, X. Qiu, R. A. Kozak, J. I. Brooks, S. Kern, A. Wolz, A. Sprecher, J. Greig, K. Lokuge, D. K. Kargbo, B. Kargbo, A. D. Caro, A. Grolla, D. Kobasa, J. E. Strong, G. Ippolito, M. V. Herp, and G. P. Kobinger, *Ebola viral load at diagnosis associates with patient outcome and outbreak evolution*, The Journal of Clinical Investigation, 125 (2015), pp. 4421–4428.
[9] P. S. Dodds and D. J. Watts, *A generalized model of social and biological contagion*, Journal of Theoretical Biology, 232 (2005), pp. 587–604.
[10] E. Estrada and J. A. Rodríguez-Velázquez, *Subgraph centrality and clustering in complex hyper-networks*, Physica A: Statistical Mechanics and its Applications, 364 (2006), pp. 581–594.
[11] A. Ganesh, L. Massoulié, and D. Towsley, *The effect of network topology on the spread of epidemics*, Proceedings - IEEE INFOCOM, 2 (2005), pp. 1455–1466.
[12] T. Gross, C. J. D. D'Lima, and B. Blasius, *Epidemic dynamics on an adaptive network*, Phys. Rev. Lett., 96 (2006).
[13] P. Hartman, *On the stability in the large for systems of ordinary differential equations*, Canadian Journal of Mathematics, 13 (1961), pp. 480–492.
[14] H. A. Herrmann and J.-M. Schwartz, *Why COVID-19 models should incorporate the network of social interactions*, Physical Biology, 17, p. 065008.
[15] D. J. Higham and H.-L. de Kergorlay, *Epidemics on hypergraphs: Spectral thresholds for extinction*, Proceedings of the Royal Society, Series A, 477 (2021).
[16] I. Iacoponi, G. Petri, A. Barrat, and V. Latora, *Simplicial models of social contagion*, Nature Communications, 10 (2019).
[17] I. Kiss, J. C. Miller, and P. L. Simon, *Mathematics of Epidemics on Networks: From Exact to Approximate Models*, Springer, Berlin, 2017.
[18] A. Koriat, S. Adiv-Mashinsky, M. Undorf, and N. Schwarz, *The prototypical majority effect under social influence*, Personality and Social Psychology Bulletin, 44 (2018), pp. 670–683.
[19] C. Kuehn and C. Bick, *A universal route to explosive phenomena*, Science Advances, 7 (2021).
[20] N. W. Landry and J. G. Restrepo, *The effect of heterogeneity on hypergraph contagion models*, Chaos, 30 (2020).
[21] N. W. Landry and J. G. Restrepo, *Hypergraph assortativity: a dynamical systems perspective*, 2022, https://arxiv.org/abs/2109.01099.
[22] P. V. Mieghem, J. Omic, and R. Kooij, *Virus spread in networks*, IEEE Transactions on Networking, 17 (2009).
[23] M. Petrovitch, *Sur une manière d'étendre le théorème de la moyenne aux équations différentielles de premier ordre*, Mathematische Annalen, 54 (1901), pp. 417–436.
[24] J. J. Torres and G. Bianconi, *Simplicial complexes: higher-order spectral dimension and dynamics*, Journal of Physics: Complexity, 1 (2020), p. 015002.
[25] D. Wang, Y. Zhao, J. Luo, and H. Leng, *Simplicial SIRS epidemic models with nonlinear incidence rates*, Chaos: An Interdisciplinary Journal of Nonlinear Science, 31 (2021), p. 053112.
[26] Y. Wang, D. Chakrabarti, C. Wang, and C. Faloutsos, *Epidemic spreading in real networks: an eigenvalue point of view*, Proceedings 22nd International Symposium on Reliable Distributed Systems, (2003).